PROCEEDINGS, 51st Workshop on Geothermal Reservoir Engineering
Stanford University, Stanford, California, February 9-11, 2026
SGP-TR-230

Thermal Management Analysis of Conventional Multi-PCB-Stack for Geothermal Drilling Tools

Gorka Plata[1], Shraddha Singh[1] and John Clegg[2]

[1]Hephae Energy Technology Europa, Bilbao, Spain, [2]Hephae Energy Technology, Houston, Texas, United States

gplata@hephaeet.com

Keywords: Geothermal, Printed Circuit Board, Thermal Management, High Temperature, Measurement-While-Drilling

ABSTRACT

Efficient thermal management of downhole electronics remains a critical challenge for the deployment of Measurement-While-Drilling (MWD) systems in high temperature geothermal environments. This study evaluates the thermal performance of conventional multilayer polyimide-based printed circuit boards (PCBs) within a modular, multi-stack architecture. Experimental tests were conducted under controlled heating conditions to characterize the temperature response and extract effective thermophysical properties of the PCB material. This data was then used to calibrate conjugate heat transfer simulations of both the PCB and the complete tool assembly. Results show that conventional PCBs exhibit anisotropic heat conduction, with radial thermal conductivities between 20–25 W/m·K, and axial values increasing from 0.3 to 0.6 W/m·K as temperature rises from 60°C to 200°C. Simulations indicate that conventional PCBs can effectively dissipate heat for low-power components (< 0.5 W) without excessive temperature rise, supporting their viability for modular MWD configurations. The findings provide valuable insights for designing cost-efficient, thermally reliable electronics suitable for next-generation geothermal drilling systems.

1. INTRODUCTION

The earth's deep heat lies everywhere beneath our feet. Geothermal energy is a renewable and baseload source of energy that represents a strategic addition to meeting the climate neutrality goals on a global scale. To meet the increasing energy demand, the geothermal sector is growing beyond conventional geothermal systems, commonly driven by tectonic zones where natural heat, water, and fluid pathways exist near the surface. To expand geothermal energy's global reach, next-generation geothermal wells with engineered reservoirs in hot dry rock provide a critical pathway to access the earth's heat economically, including opening viable geothermal localities for everyone, everywhere. Next-generation geothermal wells, including Enhanced Geothermal Systems (EGS) and Advanced Geothermal Systems (AGS), are drilled primarily to extract heat from the Earth's subsurface using horizontal drilling of wellbores as shown in Figure 1. Utah FORGE foresees the potential of EGS not being limited by traditional geothermal hotspots, with the ability to unlock heat widely across different geologies (Jones et al., 2024). Next-Generation geothermal operators are pushing the boundaries, looking to drill horizontally deeper and hotter than ever seen before, as they progress towards superhot rock temperatures at 374°C.

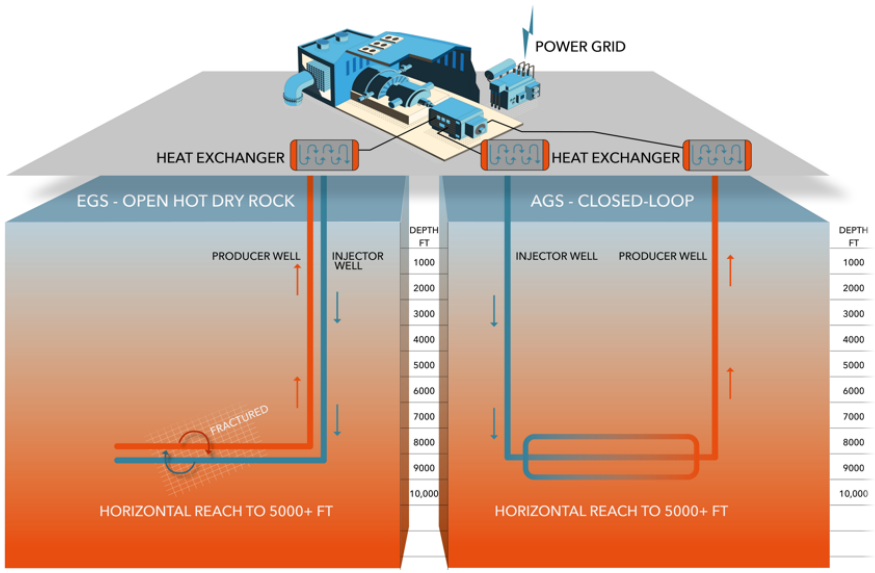

Figure 1: Next-generation geothermal systems with EGS (left) and AGS (right).

According to the Clean Air Task Force, just 1% of the world's superhot rock energy could generate 8x more energy than the rest of the world's electricity put together (Clean Air Task Force, 2025). The technology required to drill next-generation geothermal systems stems from drilling unconventional natural gas wells using intersecting technologies that include Measurement-While-Drilling (MWD) tools.

Next-generation geothermal systems typically have complex directional well profiles, often involving multiple wells drilled closely, requiring MWD technology as well.

As illustrated in Figure 1, directional drilling plays a fundamental role in both EGS and AGS configurations. Horizontal drilling is required to maximize the contact area between the circulating fluid and the geothermal formation, at depths where rock temperatures are highest. This maximized surface interaction allows the fluid to absorb sufficient heat to achieve effective system performance.

Directional drilling technologies are well established in the oil and gas industry (Ma et al., 2016), providing a mature technological foundation for their adaptation to geothermal applications. However, existing oil and gas drilling equipment typically operates only up to 175–185°C, which significantly limits its applicability to high temperature geothermal environments (Stefánsson et al., 2018). Furthermore, as highlighted by Malek et al. (2022), substantial technological advances in drilling methods are still needed with the upside of reducing drilling costs by over 50% to make geothermal electricity generation cost-competitive on a global scale. Therefore, the development of cost-effective, high temperature directional drilling equipment is critical for scaling up next-generation geothermal systems.

Achieving this requires careful thermal management design of drilling equipment, particularly to ensure that MWD electronics can withstand the combined effects of downhole heating, shock, and vibration. From a thermal perspective, two main heat sources must be considered: (1) geothermal formation heat, and (2) self-heating from the electronics. The first source necessitates effective thermal shielding to reduce heat ingress from the surroundings, while the second requires efficient heat dissipation to prevent excessive self-heating that could lead to electronic failure.

Traditionally, drilling mud has been employed to cool the equipment and dissipate formation heat (Yan et al., 2014). More recently, drill pipes with insulated coatings have been developed to further limit heat transfer from the formation to the drilling system (Vetsak et al., 2024). Regarding electronic self-heating, conventional thermal mitigation strategies typically include the use of high-conductivity heat sinks, often made of copper, to facilitate heat evacuation (Parrott et al., 2000; Peng et al., 2020; Rafie, 2007), as well as Phase Change Materials (PCMs) to absorb excess heat once a threshold temperature is reached (Lan et al., 2020; Lv et al., 2022; Peng et al., 2020; Shang et al., 2017). Some systems even combine thermal shields with passive cooling elements (such as cold masses) to both delay external heat transfer and compensate for internally generated heat (Hjelstuen et al., 2020).

While cooling techniques can be valuable in combination with higher temperature tools, cooling the entire tool is inefficient and not scalable for cost-effective, continuous drilling that must withstand prolonged exposure to high temperatures and harsh mechanical conditions. To address this limitation, an integrated approach that couples robust mechanical design with advanced thermal management is required.

It has already been proposed by the authors a novel mechanical concept that enables modular construction of drilling tools while incorporating reliable thermal management combining mud based cooling and efficient electronic heat sinking for high temperature environments (Plata et al., 2025). In this study, the modular PCB stacking approach was validated assuming ceramic PCB substrates to promote thermal transfer. However, it is still uncovered how this modular proposal could work with conventional PCBs. Hence, the following sections detail the impact of using conventional PCBs on the thermal management of the system, supported by thermal tests and simulations demonstrating the effectiveness and sensitivity of the approach.

2. METHODOLOGY

2.1 Thermal tests

The experimental campaign aimed to characterize the heat dissipation behavior of conventional polyimide-based printed circuit boards (PCBs) under controlled thermal and electrical loading. The tests consist of inserting a circular PCB into an already preheated muffle oven (up to 200ºC) while the heating element is being self-heated by an external power supply. The system was allowed to reach steady-state, typically within 3–4 minutes, before recording the stabilized temperatures. Stycast potting compound was applied to secure components and enhance thermal contact, particularly improving convective exchange on the outer surface.

The test board consisted of a circular multilayer PCB fabricated from Arlon 85N polyimide reinforced with copper foil and finished with nickel/gold (Ni/Au) plating. A resistive heating element (component R1) located at the geometric center of the PCB emulated a heat-generating electronic chip. A thermocouple was mounted at a radial position U10 to capture temperature gradient across the board, while an additional thermocouple monitored the ambient temperature within the oven chamber.

To evaluate the evolution of the thermal properties of the PCB in function of temperature, the thermal tests were carried out at 60ºC, 100ºC, 150ºC and 200ºC. Note that the selection of 60ºC was defined by the minimum temperature where the utilized thermocouples were accurate. The PCB assembly was connected to a programmable power supply delivering controlled current levels at different temperatures to avoid overheating the chip but still capturing a wide range of power input. Table 1 summarizes the power input at the different conditions.

Figure 2: Utilized test equipment to conduct thermal tests on the proposed circular conventional PCB.

Table 1: Summary of the power supplied to the heating element at different oven temperatures.

Oven temperature (ºC)	Input Current (A)	Expected input Power (W)
60	1	1.5
	1.5	3.4
	2	6
100	1	1.5
	1.5	3.4
	2	6
150	1	1.5
	1.25	2.5
	1.5	3.4
200	0.75	1
	1	1.5
	1.25	2.5

2.2 Thermal simulations of the PCB

The PCB consisted of alternating layers of Arlon 85N polyimide, copper and Ni/Au plating, meaning that the PCBs thermophysical properties are not uniquely the ones of polyimide, but the others need also to be considered. Hence, by volumetric averaging of the constituent layers, considering the respective thickness ratios used in the manufactured board, the following are the determined equivalent thermophysical properties:

Table 2: Estimated equivalent thermophysical properties of the conventional PCB.

Property	Symbol	Value	Units
Density	ρ	2175	kg/m³
Specific Heat Capacity	Cp	1461	J/kg·K
Thermal Conductivity	K	0.24	W/m·K

These equivalent PCB material properties have been used as an initial point to develop in SimScale a digital twin by back engineering the experimental result. Regarding the digital twin itself, the Conjugate Heat Transfer (CHT) module has been utilized to model the thermal behavior of the PCB by replicating the experimental boundary conditions and heating configuration (natural convection oven). The PCB was meshed using the immersed-boundary method with local refinement around the heating component and thermocouple regions. Simulations were performed under steady state conditions until residuals converged below 1×10^{-6}. The objective was to extract effective

equivalent thermal properties for the conventional PCB and validate them against experimental data before integrating them into the multi-stack tool simulations.

2.3 Thermal simulations of the tool

The tool level simulations followed the methodology detailed by Plata et al. (2025) adapting it to incorporate the thermal characteristics of the conventional PCB derived from the previous experimental and thermal analyses. The modeled geometry reproduced the modular axially stacked configuration of circular PCBs, metallic crowns and bases, guiding rails, a spring sleeve, and external pressure housing (Figure 3).

The simulation domain included up to four stacked PCBs, each with a central heat-generating chip of size 11.5 × 11.5 mm. The external mud cooled bulkhead served as the main heat sink, while the annular space between the electronic housing and the pressure vessel was assumed to be stagnant air. Radial surfaces in contact with drilling mud were assigned a convective heat-transfer coefficient (CHTC) of 1000 W/m²K and a mud temperature of 210°C, consistent with the geothermal drilling scenario used in the ceramic-PCB study.

Material properties for non-PCB components were identical to those in Plata et al. (2025): aluminum for crowns, bases, guides, and sleeve; BeCu for the bulkhead; stainless steel for the housing; and high temperature silicone rubber for insulation. For simplicity, all contact interfaces were assumed to be perfect. Steady state simulations were run for chip power inputs of 0.25, 0.5, 0.75, and 1 W and for 1–4 PCB stack configurations. The same mesh refinement and convergence criteria were applied (Plata et al., 2025).

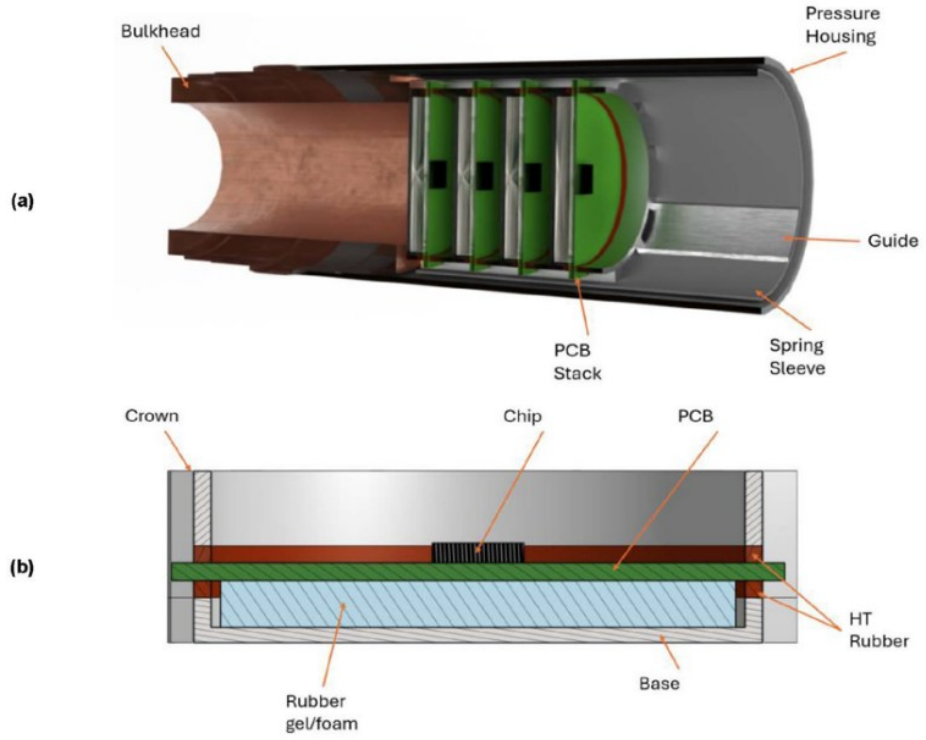

Figure 3: Schematic of (a) proposed multi-stack electronics housing and (b) proposed PCB stack assembly (Plata et al., 2025).

3. RESULTS AND DISCUSSION

3.1 Thermal tests

An example of the registered temperature evolution over time during the experimental tests is shown in Figure 4. It can be seen how the temperature reaches a steady state and how repetitive the results are. Table 3, Figure 5 and Figure 6 show the registered experimental values and a comparison of the experimental results.

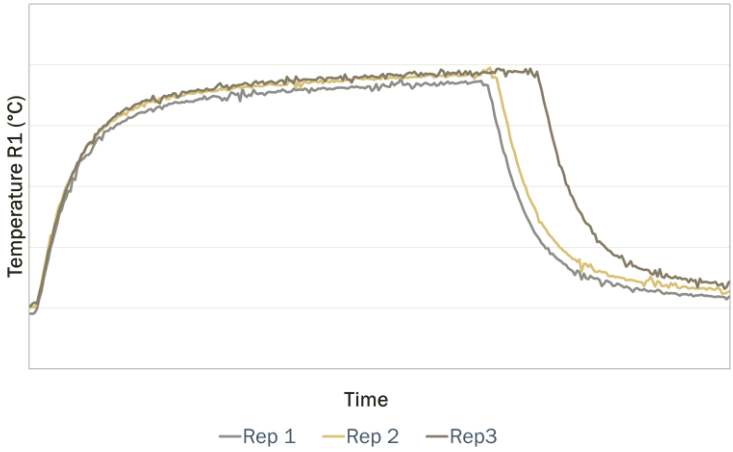

Figure 4: Temperature-time curve for R1 (chip) at ambient temperature of 60ºC and a supplied power of 1.5 W.

Table 3: Summary of the registered temperatures in the different locations of the PCB.

Oven temperature (ºC)	Input Power (W)	R1 (ºC)		U10 (ºC)	
		T	ΔT	T	ΔT
60	1.5	98.9	38.9	64.9	4.9
	3.4	143.7	83.7	70.1	10.1
	6	203.1	143.1	77.4	17.4
100	1.5	135.3	35.3	103.4	3.4
	3.4	177.8	77.8	108	8
	6	232.7	132.7	114	14
150	1.5	183.2	33.2	153	3
	2.5	200.9	50.9	154.4	4.4
	3.4	222.8	72.8	156.4	6.4
200	1	218.6	18.6	201.9	1.9
	1.5	231.8	31.8	202.9	2.9
	2.5	249.2	49.2	204.2	4.2

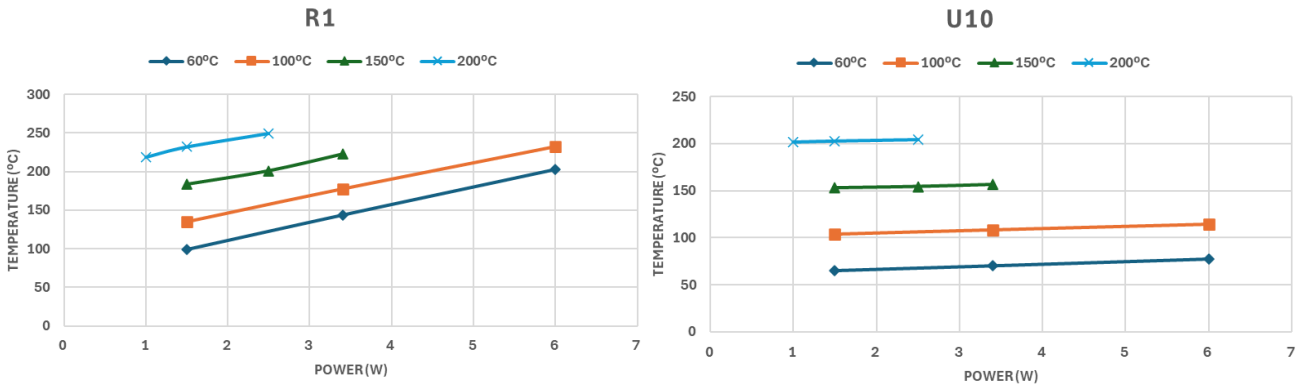

Figure 5: Temperature-Power plot for R1 (chip) and U10 (PCB) at different ambient temperatures.

The results show the influence of the power on the heating of chip (R1), having an overheating difference ranging from ~17ºC (200ºC and 1W condition) to ~126ºC (60ºC and 6W condition) with respect to the overheating registered in a radial position of the PCB (U10). These findings highlight the limitations of the PCB in efficiently conducting and dissipating heat under high-power operating conditions. In any case, there are signs of radial heat evacuation that might be enough to work at low power conditions.

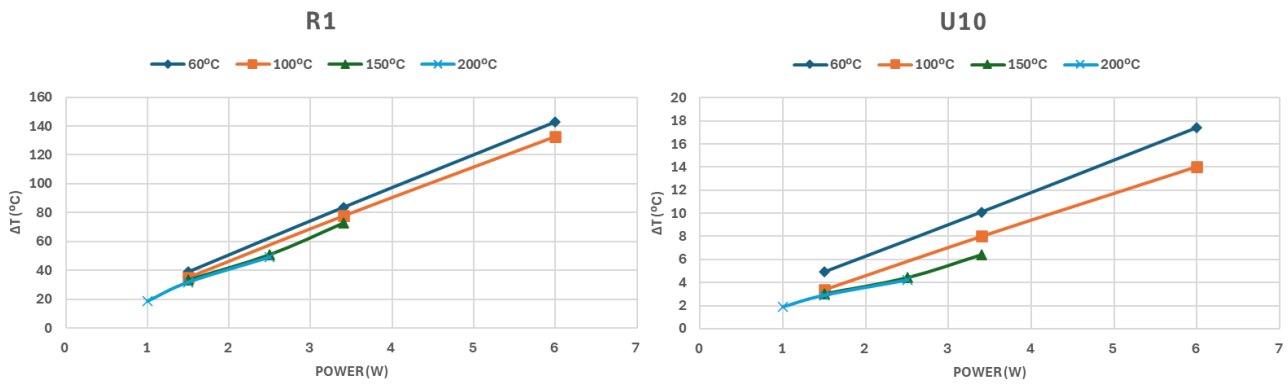

Figure 6: Overheating-Power plot for R1 (chip) and U10 (PCB) at different ambient temperatures.

The experimental data also revealed that the chip (R1) and PCB (U10) temperature increases linearly with input power at constant ambient temperature, while the slope of the curve decreases at high ambient temperatures (≥ 200°C) (Figure 7). This reduction in slope might be attributed to the temperature-dependent thermal properties of the chip and different PCB layer materials. As a result, there seems to be an increase in conductivity, density, and/or specific heat with temperature, therefore reducing the generated overheating for the same power conditions at higher temperatures.

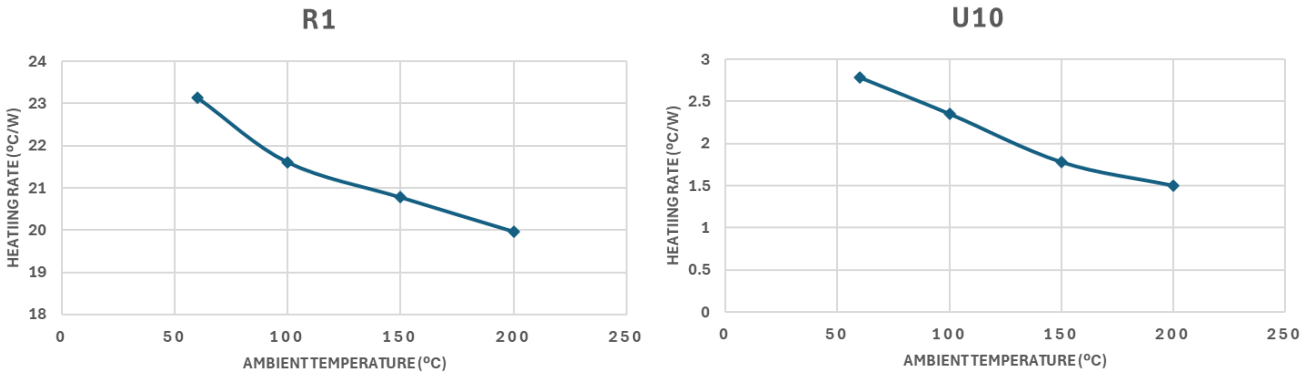

Figure 7: Heating rate ambient temperature plot for R1 (chip) and U10 (PCB).

3.2 Thermal simulations of the PCB

Using the experimental data as a basis, simulations were carried out to reverse engineer the PCB's thermal properties under the tested operating conditions. Based on the initial PCB's thermal properties shown in Table 2, the analysis has been focused on determining the thermal conductivity (K) in order to match the experimental results. After several iterations, the following are the determined values:

Table 4: Summary of the reverse engineered effective thermal conductivities of the PCB for the different ambient temperatures.

Temperature (°C)	Average Kx/Ky	Average Kz
60	25	0.3
100	23	0.4
150	22	0.5
200	20	0.6

As can be observed from Table 4, the PCB shows an anisotropic thermal conductivity pattern due to its layered multi-material structure. The simulated results suggest that the radial dissipation of the heat is greater than the axial one. These results are expected, as the heat must traverse multiple material layers, with polyimide comprising the largest proportion. On the contrary, once the temperature reaches axially to a copper or Ni/Au layer, the temperature can travel radially through that layer at the thermal conductivity of that specific material. Hence, these results show the capacity of the conventional PCBs to partially act as a radial heat sink, being the efficiency dependent on its multilayered structure.

Apart from that, the results also suggest a reduction in the reverse engineered radial thermal conductivity and an increase in the axial thermal conductivity. While these results confirm the temperature dependence of the PCB material thermal properties, consistent with the experimental observations, the derived values should be considered representative only of this specific setup due to two influencing factors. First, the density and specific heat values have maintained constant for convergence simplicity, which means that the effect of their variation is assumed into these reverse engineered values. Second, because the thermal properties of the polyimide increase with temperature (Kurabayashi et al., 1999), enhancing the axial heat evacuation, the amount of heat that needs to be evacuated radially is reduced, showing a reduction in the reverse engineered radial conductivity value that is related to the experimental setup.

In order to have more realistic effective conductivity values that could be used with other boundary conditions, more experimental tests should be carried out, not only registering the top surface of the PCB, but also the bottom one. This process is critical to gain a sense of the effect of the axial thermal conductivity, together with additional simulations that consider the density and specific heat variations in function of temperature. In any case, these reverse engineered values are good enough for the sensitivity analysis of the proposed modular tool, as the overall boundary conditions are similar to the experimental ones between R1 and U10.

3.3 Thermal simulations of the tool

The results of the different simulations at 210ºC are summarized in Table 5-8. There, we can observe the registered maximum temperatures on the electronic chip per PCB stack and power where the trend clearly shows that the higher the power and/or the number of PCB stacks, the higher the self-heating of the electronic element. This trend is also visible in Figure 8, where the temperature evolution per number of stacks and power of the chip is shown.

Table 5: Summary of the maximum registered temperatures in the performed simulation with 0.25 W input power on each chip.

Nº of stacks	Temperature (ºC)			
	Chip 1	Chip 2	Chip 3	Chip 4
1	213.4			
2	213.4	213.9		
3	213.5	213.9	214.2	
4	213.5	214	214.3	214.5

Table 6: Summary of the maximum registered temperatures in the performed simulation with 0.5 W input power on each chip.

Nº of stacks	Temperature (ºC)			
	Chip 1	Chip 2	Chip 3	Chip 4
1	216.8			
2	216.9	217.7		
3	216.9	217.8	218.4	
4	217	217.9	218.5	219.1

Table 7: Summary of the maximum registered temperatures in the performed simulation with 0.75 W input power on each chip.

Nº of stacks	Temperature (ºC)			
	Chip 1	Chip 2	Chip 3	Chip 4
1	220.2			
2	220.3	221.6		
3	220.4	221.7	222.6	
4	220.5	221.9	222.6	223.6

Table 8: Summary of the maximum registered temperatures in the performed simulation with 1 W input power on each chip.

Nº of stacks	Temperature (ºC)			
	Chip 1	Chip 2	Chip 3	Chip 4
1	223.6			
2	223.7	225.4		
3	223.9	225.6	226.8	
4	224	225.8	227	228.2

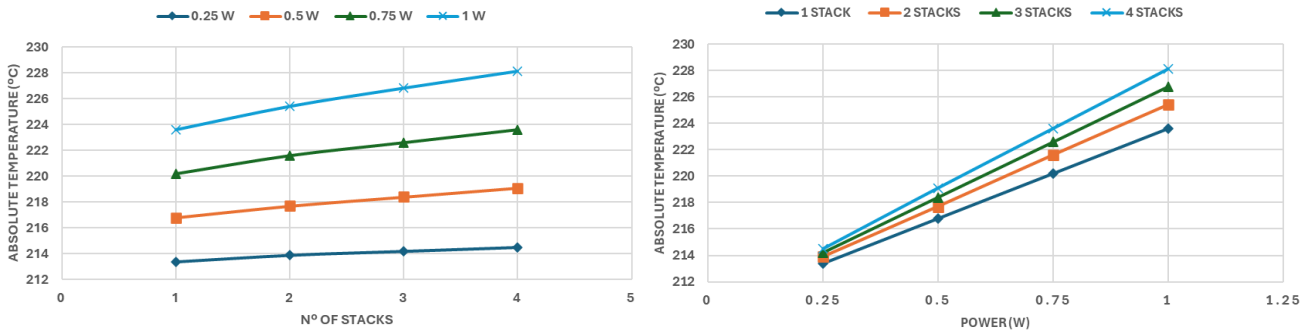

Figure 8: Simulated results showing the influence of the stack amount on the maximum temperature per power (left) and power influence on the maximum temperature per PCB Stack (right).

From the simulations results, it can be clearly seen how at a realistic working condition (0.5W) the maximum registered overheating would be around 7-9 ºC, showing the capacity of using conventional PCBs for low power conditions. Moreover, as shown in Figure 9, increasing the number of stacks does not lead to a significant rise in the recorded maximum temperatures, indicating the effectiveness of the proposed modular design even when implemented with conventional PCBs. In contrast, power has a much stronger impact on chip overheating, with small changes in supplied power producing effects an order of magnitude greater than those associated with the number of stacks.

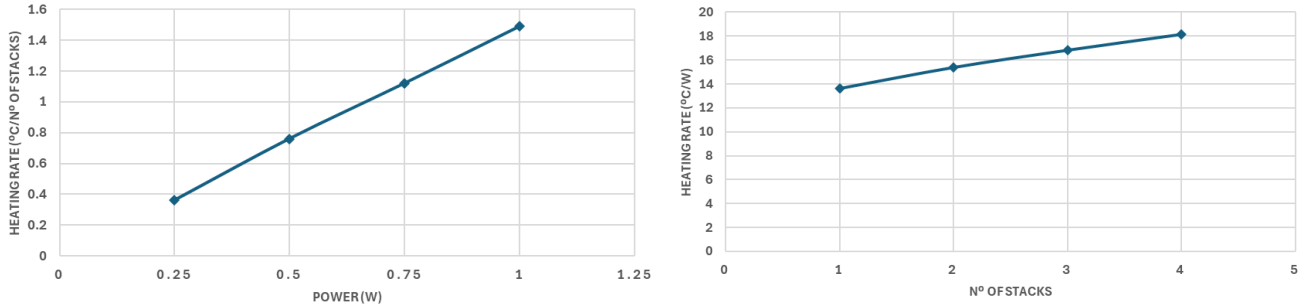

Figure 9: Simulated results showing the influence of the heating rate (ºC/W) on the maximum temperature per number of stacks (left) and the influence of heating rate (ºC/Nº of stacks) on the maximum temperature per power (right).

3.4 Discussion

The results confirm that conventional PCBs, when integrated with the proposed structural design, can effectively dissipate heat from low power electronic components, while maintaining a modular and easily assembled configuration. Nevertheless, given the theoretical nature of this study, certain limitations must be acknowledged. In particular, all interfaces between components were assumed to exhibit perfect thermal contact. In practice, surface irregularities may introduce contact resistances that slightly reduce overall heat transfer efficiency. However, since each stack in the assembly is subjected to a defined preload, the assumption of near perfect contact is considered reasonable for the purposes of this analysis.

Regarding the experimental results on the conventional PCB, access was limited to the top surface due to the constraints of the test setup. To obtain a more comprehensive understanding of the PCB's thermal profile, future tests should incorporate thermocouples at multiple locations, including the bottom surface and internal layers. This would enable a more accurate estimation of the PCB's effective thermophysical properties.

The effective thermal properties estimated through reverse engineering were derived by independently calculating the radial and axial thermal conductivities to simplify the analysis and facilitate convergence. However, this method introduces an inherent approximation, as it assumes constant density and specific heat capacity. Moreover, the estimated conductivities are specific to this PCB design, since the layer distribution strongly influences the overall thermal behavior. A more accurate representation could be achieved by explicitly meshing each individual layer and treating the PCB as a multilayered structure. Nevertheless, this approach was deemed impractical due to the small layer thicknesses (25–500 µm) and the associated computational cost.

Finally, the simulation results of the conventional multi-PCB stack, considering the same assumptions discussed in Plata et al. (2025), show a thermal trend comparable to that of the ceramic PCBs. While the heating rate for the ceramic PCB was estimated to be between 5.5 and 6.9°C/W, the corresponding rate for the conventional PCB ranges between 13.5 and 18°C/W, approximately two to three times higher. A similar tendency is observed in relation to the number of stacks: the heating rate increases from 0.2–0.7°C/stack for the ceramic

PCB to 0.35–1.5°C/stack for the conventional one, again about twice as high. Interestingly, the improvement achieved with ceramic substrates is smaller than might be expected based solely on their thermal conductivity difference (180 W/m·K for ceramic vs. ~20 W/m·K estimated radially for conventional PCBs). This suggests that optimizing the layer composition and architecture of conventional PCBs could substantially enhance thermal management performance, while maintaining compatibility with standard materials and manufacturing processes.

4. CONCLUSIONS

This study demonstrates that conventional polyimide-based PCBs, when incorporated into the proposed modular stack architecture, are capable of providing sufficient thermal management for low power MWD electronics in geothermal drilling environments. The key conclusions are summarized below:

- Experimental and numerical analyses confirmed anisotropic thermal behavior of the conventional polyimide-based PCB, with higher radial than axial conductivity (20–25 W/m·K vs. 0.3–0.6 W/m·K).
- Simulations show that, under realistic downhole power loads (≈0.5 W per chip), overheating remains below 10°C, validating the feasibility of the design.
- The heating rate of conventional PCBs is about two to three times higher than that of ceramic PCBs, yet the influence of stack number is minor, highlighting the robustness of the modular concept.

REFERENCES

Clean Air Task Force. 2025. Superhot Rock Geothermal Heat Mapping. Clean Air Task Force Mapping Report, https://www.catf.us/superhot-rock/heat-mapping/. Accessed 22 December 2025.

Hjelstuen, M. B., Høvik, T., Andersen, G., Volland, K., & Røed, M. H. 2021. Cryogenic Cooling Enabling Increased Performance of Logging Tools Utilizing Vacuum Flasks. Presented at. World Geothermal Congress 2020 and 2021, Reykjavik, Iceland, 24-27 October.

Jones, Clay G., Simmons, S., & Moore, J. 2024. Geology of the Utah Frontier Observatory for Research in Geothermal Energy (FORGE) Enhanced Geothermal System (EGS) Site. *Geothermics*, vol. 122, 2024, article no. 103054, https://doi.org/10.1016/j.geothermics.2024.103054

Kurabayashi, K., Asheghi, M., Touzelbaev, M., & Goodson, K. E. 1999. Measurement of the Thermal Conductivity Anisotropy in Polyimide Films. IEEE JOURNAL OF MICROELECTROMECHANICAL SYSTEMS, 8(2). https://doi.org/10.1109/84.767114

Lan, W., Zhang, J., Peng, J., Ma, Y., Zhou, S., & Luo, X. 2020. Distributed thermal management system for downhole electronics at high temperature. Applied Thermal Engineering 180: 115853. https://doi.org/10.1016/j.applthermaleng.2020.115853

Lv, Y.-G., Chu, W.-X., & Wang, Q.-W. 2022. Thermal Management Systems for Electronics Using in Deep Downhole Environment: A Review. International Communications in Heat and Mass Transfer 139: 106450. https://doi.org/10.1016/j.icheatmasstransfer.2022.106450

Ma, T., Chen, P., & Zhao, J. 2016. Overview on vertical and directional drilling technologies for the exploration and exploitation of deep petroleum resources. Geomechanics and Geophysics for Geo-Energy and Geo-Resources 2 (4):365–395. https://doi.org/10.1007/s40948-016-0038-y

Malek, A. E., Adams, B. M., Rossi, E., Schiegg, H. O., & Saar, M. O. 2022. Techno-economic analysis of Advanced Geothermal Systems (AGS). Renewable Energy, 186: 927–943. https://doi.org/10.1016/j.renene.2022.01.012

Parrott, R. A., Song, H., & Chen, K. C. 2000. Cooling System for Downhole Tools. International (PCT) Patent No. WO/2000/045099A2.

Peng, J., Lan, W., Wang, Y., Ma, Y., & Luo, X. 2020. Thermal Management of the High-power Electronics in High Temperature Downhole Environment. Proc. IEEE 22nd Electronics Packaging Technology Conference. 369–375.Singapore, Singapore, 02-04 December, 7 pages. https://doi.org/10.1109/EPTC50525.2020.9315026

Plata, G., Singh, S., & Clegg, J. 2025. Effect of Modularity on the Thermal Management of Optimized Printed Circuit Boards for Geothermal Drilling Tools. SPE - International Association of Drilling Contractors Drilling Conference Proceedings, 2025-March. https://doi.org/10.2118/223773-MS

Rafie, S. 2007. Thermal management of downhole oil & gas logging sensors for high temperature high pressure applications using nanoporous materials. Proc., 2nd Energy Nanotechnology International Conference. 27-32. Santa Clara, California, USA, 5-7September, 6 pages. https://doi.org/10.1115/ENIC2007-45007

Shang, B., Ma, Y., Hu, R., Yuan, C., Hu, J., & Luo, X. 2017. Passive thermal management system for downhole electronics in harsh thermal environments. Applied Thermal Engineering 118: 593–599. https://doi.org/10.1016/j.applthermaleng.2017.01.118

Stefánsson, A., Orka, H. S., Duerholt, R., Schroder, J., Macpherson, J., Hohl, C., Kruspe, T., Eriksen, T.-J., & Hughes, B. 2018. A 300 Degree Celsius Directional Drilling System. Presented at IADC/SPE Drilling Conference and Exhibition,6–8 March. https://doi.org/10.2118/189677-MS

Vetsak, A., Besoiu, C., Zatonski, V., Torre, A., Hodder, M., & Toews, M. 2024. The Insulated Drill Pipe – Field Experienceand Thermal Model Validation. Presented at IADC/SPE International Drilling Conference and Exhibition, 5-7 March. https://doi.org/10.2118/217753-MS

Yan, C., Deng, J., Yu, B., Li, W., Chen, Z., Hu, L., & Li, Y. 2014. Borehole Stability in High-Temperature Formations. Rock Mechanics and Rock Engineering 47 (6): 2199–2209. https://doi.org/10.1007/s00603-013-0496-2